Plane hybrid stress elements for 3D analysis of moderately thick solids subjected to loading symmetric to midsurface

Q.Z. Xiao, M. Dhanasekar *

Centre for Railway Engineering, Central Queensland University, Rockhampton, QLD 4702, Australia

Abstract

Plane semi-analytical hybrid stress elements are formulated from the 3D Hellinger–Reissner principle for modelling moderately thick structural components with and without hollows subjected to loadings symmetric to the midsurface. These components possess symmetry in the thickness direction but could not be idealised as either plane stress or plane strain problems. 3D displacement and stress fields conforming to the exact plane stress solution are assumed and normal stresses on the surfaces parallel to the thickness direction are nullified. These 2D elements possess good convergence characteristics and simulate the 3D behaviour of solids whose stress free surfaces exhibit negligible out-of-plane distortion with good level of accuracy comparable to 3D analyses by ABAQUS.
© 2006 Elsevier Ltd. All rights reserved.

Keywords: Semi-analytical hybrid stress element; Solids symmetric to midsurface; 3D Hellinger–Reissner principle; Optimisation of hybrid stress element

1. Introduction

Structural analysts resort to 3D modelling of the components or structures that are moderately thick although they are subjected to in-plane loading and their lateral surfaces remain traction free. For the illustration of such cases, several examples could be drawn from civil engineering application, namely, the modelling of shear walls of varying thickness (Foster and Rangan, 1999) and simple prisms used for the quality control of concrete and masonry construction (Afshari and Kaldjian, 1989). These problems could not be commonly analysed using the classical plane strain or plane stress approach and a full 3D analysis is essential for the accurate prediction of all stress and displacement components.

Plane stress is used for problems involving small thickness relative to in-plane dimensions and free lateral boundary conditions. Plane strain, on the other hand, is suitable where the thickness of the solid is much larger than other characteristic dimensions. Under plane strain assumption, equilibrium, compatibility and constitutive equations are precisely satisfied. Unfortunately, not all the compatibility conditions are satisfied in the

---

* Corresponding author. Tel.: +61 7 4930 9677; fax: +61 7 4930 6984.
E-mail address: m.dhanasekar@cqu.edu.au (M. Dhanasekar).

plane stress approach because it supposes that all variables are independent of z-axis (an axis oriented along the thickness direction), and all out-of-plane stress components are identically equal to zero ($\sigma_z = \tau_{yz} = \tau_{zx} = 0$) (Timoshenko and Goodier, 1970) throughout the thickness of the body. In order to model structural components of moderate thickness, in this paper we have considered that the out-of-plane stress components vanish at all external lateral planes normal to the z-axis (in other words, these stresses remain non-zero within the body). This consideration necessitated all fields be kept as functions of x, y and z.

Timoshenko and Goodier (1970) proposed a 3D exact solution for plane stress problems with the assumption of $\sigma_z = \tau_{yz} = \tau_{zx} = 0$ using a stress function ϕ that depends on x, y and z. The theory validates the classical plane stress assumption for solids possessing infinitesimal thickness but still is inadequate for problems with moderate thickness (or, bodies whose dimensions are comparable to each other). Ye (1997) proposed an alternative exact formulation by adopting the assumptions $\tau_{yz} = \tau_{zx} = 0$, and $\sigma_z = \sigma_z(x, y)$ as a harmonic function satisfying the condition $\sigma_{z,xx} + \sigma_{z,yy} = 0$ and formulated a 2D displacement element capable of predicting the out-of-plane normal stress σ_z. However, his method has not satisfied the traction free conditions on the free lateral surfaces of the solids. This paper presents 2D hybrid stress element formulation that satisfies the traction free conditions on all free lateral surfaces of the solids.

Theoretically the analysis of the plane deformable bodies possessing moderate thickness belongs neither to the classical plane strain/stress theories nor to the modified plane stress theories. Similar problems occur in the evaluation of the stress intensity factor in fracture mechanics (Broek, 1982; Zhou and Hsieh, 1988). For these problems, analysis based on 3D modelling is expected to yield precise results but it is not only computationally expensive, but also complicated for mesh generation and interpretation of the output data. In this paper we report four-noded quasi-3D hybrid stress elements with 24 stress parameters, represented by Q3D24β for non-hollow bodies, and Q3D24βH for hollow bodies, formulated using the 3D Hellinger–Reissner principle for the modelling of solids and structural components of moderate thickness, or bodies whose dimensions are comparable to each other.

In the formulation the displacement and stress fields along the thickness direction are represented analytically by improving the modified plane stress theory proposed by Timoshenko and Goodier (1970) and Ye (1997). However, unlike the modified plane stress theories, the hybrid stress element reported in this paper has the potential to predict non-zero out-of-plane stress components within the body. The element satisfies the equilibrium, compatibility and constitutive equations in a variational sense (weak form). As stress-free conditions are enforced at the external lateral surfaces in the formulation, the element would precisely predict the behaviour of thick solids whose external lateral surfaces do not undergo out-of-plane distortion.

Numerical results for illustrating the h-refinement, and aspect ratio sensitivity to the convergence rate and the accuracy of the element are presented. The results are compared with that of 3D elements available in ABAQUS where required.

2. 3D displacement and stress fields for in-plane actions of a solid

Consider a solid that has a symmetry plane xy as shown in Fig. 1. The loads are also symmetric to the xy-plane. The z-axis is along the thickness direction as in Fig. 1. According to the exact theory of the plane stress
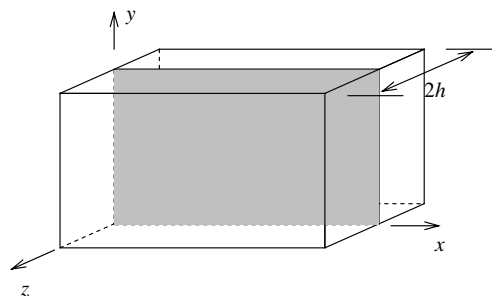

Fig. 1. A symmetric solid.

state, in order to meet all the compatibility conditions for plane stress deformation, a quadratic term in z that vanishes when the thickness reaches zero must be included to the traditional Airy's stress function (Timoshenko and Goodier, 1970; Ye, 1997). Also the functions of the in-plane displacement components that are independent of the coordinate z must be allowed to vary in the z-direction. Thus the in-plane displacement components which are symmetry to the midsection xy are represented by the following functions

$$u(x, y, z) = u_0(x, y) + z^2 u_1(x, y) \tag{1a}$$
$$v(x, y, z) = v_0(x, y) + z^2 v_1(x, y) \tag{1b}$$

and the lateral displacement which is anti-symmetric to the midsection xy is assumed as

$$w(x, y, z) = z w_0(x, y) + z^3 w_1(x, y) \tag{1c}$$

Ye (1997), however, assumed the lateral displacement $w(x, y, z) = z w_0(x, y)$ without the cubic term. In the absence of the cubic z term the traction free condition on the lateral surfaces cannot be precisely satisfied.

With the displacement modes (1) we obtain the following in-plane strain components:

$$\varepsilon_x = u_{0,x} + z^2 u_{1,x}$$
$$\varepsilon_y = v_{0,y} + z^2 v_{1,y} \tag{2a}$$
$$\gamma_{xy} = (u_{0,y} + v_{0,x}) + z^2 (u_{1,y} + v_{1,x})$$

We also obtain the following out-of-plane strain components:

$$\gamma_{yz} = z(w_{0,y} + 2v_1) + z^3 w_{1,y}$$
$$\gamma_{zx} = z(w_{0,x} + 2u_1) + z^3 w_{1,x} \tag{2b}$$
$$\varepsilon_z = w_0 + 3z^2 w_1$$

In both (2a) and (2b), $(\ )_{,i} = \partial / \partial x_i$.

Stresses are easily calculated from strains given in Eqs. (2a) and (2b) using Hooke's law. Out-of-plane normal stress σ_z is a quadratic function of z and symmetric to the midsection xy, and shear stresses τ_{yz} and τ_{zx} are cubic functions of z and anti-symmetric to the midsection xy. However, these exact stresses compatible with the displacements (1) are generally not able to satisfy the traction free condition on the lateral surfaces. This condition is essential for the accurate solution of plane deformable bodies with moderate thickness (i.e., solids whose dimensions are comparable to each other). Since our purpose is to develop a universal hybrid stress element method, we will not use these exact stresses in the element formulation. In stead, we will adopt assumed stresses that have the main features (symmetry or anti-symmetry to the midsection xy) of the exact stresses and satisfy the traction free condition on the lateral surfaces.

The in-plane stress components are assumed as shown in (3a):

$$\sigma_x(x, y, z) = \sigma_{x0}(x, y) + \bar{z}^2 \sigma_{x1}(x, y)$$
$$\sigma_y(x, y, z) = \sigma_{y0}(x, y) + \bar{z}^2 \sigma_{y1}(x, y) \tag{3a}$$
$$\tau_{xy}(x, y, z) = \tau_{xy0}(x, y) + \bar{z}^2 \tau_{xy1}(x, y)$$

For exact formulation of plane deformable bodies with moderate thickness (i.e., solids whose dimensions are comparable to each other), σ_z should be a function of z because as the thickness tending to be negligibly small, σ_z should vanish. According to the equilibrium equation in the z-direction, τ_{yz} and τ_{zx} can not be zero everywhere but should be functions of (x, y, z). Note that the deformation is symmetric to the midsection, the out-of-plane stress components are, therefore, assumed as shown in (3b):

$$\tau_{yz}(x, y, z) = (\bar{z} - \bar{z}^3) \tau_{yz0}(x, y) + (\bar{z}^3 - \bar{z}^5) \tau_{yz1}(x, y)$$
$$\tau_{zx}(x, y, z) = (\bar{z} - \bar{z}^3) \tau_{zx0}(x, y) + (\bar{z}^3 - \bar{z}^5) \tau_{zx1}(x, y) \tag{3b}$$
$$\sigma_z(x, y, z) = (1 - \bar{z}^2) \sigma_{z0}(x, y) + (\bar{z}^2 - \bar{z}^4) \sigma_{z1}(x, y)$$

where $\bar{z} = \frac{z}{h}$ and h is the half thickness of the body as shown in Fig. 1. The higher order terms relevant to τ_{yz1}, τ_{zx1} and σ_{z1} are necessary for suppressing the spurious modes of the element as discussed later in this paper. Eq. (3b) define the stresses that satisfy the traction free condition on the lateral surfaces.

In the assumed displacement fields (1), the non-zero displacement components that result in vanishing strain fields (i.e., rigid deformation modes) are $u_0(x, y)$, and $v_0(x, y)$. To achieve static equilibrium, we therefore require only three prescribed displacement components in the xy-plane of the solid. In other words the number of rigid body motion modes is three. This requirement is similar to any plane element formulation although Q3D24β represents 3D stress and displacement fields.

3. Hybrid stress element formulation using Hellinger–Reissner principle

We formulate the hybrid stress element by using the 2-field Hellinger–Reissner principle with the following elemental functional (Pian and Wu, 1988; Wu and Bufler, 1991; Wu and Cheung, 1995)

$$\Pi_{\mathrm{HR}}^{(e)}(\mathbf{u}, \boldsymbol{\sigma}) = \int_{-h}^{h} \left\{ \int_{A^{(e)}} \left[-\frac{1}{2} \boldsymbol{\sigma}^{\mathrm{T}} \mathbf{S} \boldsymbol{\sigma} + \boldsymbol{\sigma}^{\mathrm{T}}(\mathbf{Du}) \right] \mathrm{d}A - \int_{A^{(e)}} \bar{\mathbf{f}}^{\mathrm{T}} \mathbf{u} \, \mathrm{d}A - \int_{S_\sigma^{(e)}} \overline{\mathbf{T}}^{\mathrm{T}} \mathbf{u} \, \mathrm{d}s \right\} \mathrm{d}z \tag{4}$$

where $\mathbf{u} = \begin{bmatrix} u & v & w \end{bmatrix}^{\mathrm{T}}$ and $\boldsymbol{\sigma} = \begin{bmatrix} \sigma_x & \sigma_y & \tau_{xy} & \tau_{yz} & \tau_{zx} & \sigma_z \end{bmatrix}^{\mathrm{T}}$. $\mathbf{S}$ is the compliance matrix, $\mathbf{D}$ the differential operator matrix

$$\mathbf{S} = \frac{1}{E} \begin{bmatrix} 1 & & & & & \\ -v & 1 & & & \text{sym} & \\ 0 & 0 & 2(1+v) & & & \\ 0 & 0 & 0 & 2(1+v) & & \\ 0 & 0 & 0 & 0 & 2(1+v) & \\ -v & -v & 0 & 0 & 0 & 1 \end{bmatrix}, \quad \mathbf{D} = \begin{bmatrix} \dfrac{\partial}{\partial x} & 0 & 0 \\ 0 & \dfrac{\partial}{\partial y} & 0 \\ \dfrac{\partial}{\partial y} & \dfrac{\partial}{\partial x} & 0 \\ 0 & \dfrac{\partial}{\partial z} & \dfrac{\partial}{\partial y} \\ \dfrac{\partial}{\partial z} & 0 & \dfrac{\partial}{\partial x} \\ 0 & 0 & \dfrac{\partial}{\partial z} \end{bmatrix}$$

$A^{(e)}$ is the area of element 'e', $S_\sigma^{(e)}$ the part of the element boundary on which traction is prescribed. $\overline{\mathbf{T}}$ and $\bar{\mathbf{f}}$ are the surface and volumetric force vector, respectively.

Consider an element with n nodes and six degrees of freedom at each node. The displacement of the element $\mathbf{u}$ is related to nodal values $\mathbf{q}$ via the shape functions $\mathbf{N}$

$$\mathbf{u} = \mathbf{Nq} \tag{5}$$

in which,

$$\mathbf{q}^{\mathrm{T}} = \lfloor \mathbf{q}^{(1)^{\mathrm{T}}} \quad \mathbf{q}^{(2)^{\mathrm{T}}} \quad \cdots \quad \mathbf{q}^{(n)^{\mathrm{T}}} \rfloor$$
$$\mathbf{N} = \begin{bmatrix} \mathbf{N}^{(1)} & \mathbf{N}^{(2)} & \cdots & \mathbf{N}^{(n)} \end{bmatrix}$$

The nodal values and shape functions for an arbitrary node i are

$$\mathbf{q}^{(i)^{\mathrm{T}}} = \begin{bmatrix} u_0^{(i)} & u_1^{(i)} & v_0^{(i)} & v_1^{(i)} & w_0^{(i)} & w_1^{(i)} \end{bmatrix} \tag{6}$$

$$\mathbf{N}^{(i)} = \begin{bmatrix} N_i & z^2 N_i & 0 & 0 & 0 & 0 \\ 0 & 0 & N_i & z^2 N_i & 0 & 0 \\ 0 & 0 & 0 & 0 & z N_i & z^3 N_i \end{bmatrix} \tag{7}$$

here $u_0^{(i)}, v_0^{(i)}, w_0^{(i)}$ and $u_1^{(i)}, v_1^{(i)}, w_1^{(i)}$ are respective values of terms u_0, v_0, w_0 and u_1, v_1, w_1 in the displacement polynomials given in Eq. (1) at node i.

The strain array relevant to Eq. (5) is

$$\boldsymbol{\varepsilon} = \mathbf{D}\mathbf{u} = \mathbf{B}\mathbf{q} \tag{8}$$

where $\mathbf{B} = [\,\mathbf{B}^{(1)} \quad \mathbf{B}^{(2)} \quad \cdots \quad \mathbf{B}^{(n)}\,]$. For an arbitrary node i

$$\mathbf{B}^{(i)} = \mathbf{B}_0^{(i)} + z\mathbf{B}_1^{(i)} + z^2\mathbf{B}_2^{(i)} + z^3\mathbf{B}_3^{(i)} \tag{9}$$

and

$$\mathbf{B}_0^{(i)} = \begin{bmatrix} N_{i,x} & 0 & 0 & 0 & 0 & 0 \\ 0 & 0 & N_{i,y} & 0 & 0 & 0 \\ N_{i,y} & 0 & N_{i,x} & 0 & 0 & 0 \\ 0 & 0 & 0 & 0 & 0 & 0 \\ 0 & 0 & 0 & 0 & 0 & 0 \\ 0 & 0 & 0 & 0 & N_i & 0 \end{bmatrix}, \quad \mathbf{B}_1^{(i)} = \begin{bmatrix} 0 & 0 & 0 & 0 & 0 & 0 \\ 0 & 0 & 0 & 0 & 0 & 0 \\ 0 & 0 & 0 & 0 & 0 & 0 \\ 0 & 0 & 0 & 2N_i & N_{i,y} & 0 \\ 0 & 2N_i & 0 & 0 & N_{i,x} & 0 \\ 0 & 0 & 0 & 0 & 0 & 0 \end{bmatrix}$$

$$\mathbf{B}_2^{(i)} = \begin{bmatrix} 0 & N_{i,x} & 0 & 0 & 0 & 0 \\ 0 & 0 & 0 & N_{i,y} & 0 & 0 \\ 0 & N_{i,y} & 0 & N_{i,x} & 0 & 0 \\ 0 & 0 & 0 & 0 & 0 & 0 \\ 0 & 0 & 0 & 0 & 0 & 0 \\ 0 & 0 & 0 & 0 & 0 & 3N_i \end{bmatrix}, \quad \mathbf{B}_3^{(i)} = \begin{bmatrix} 0 & 0 & 0 & 0 & 0 & 0 \\ 0 & 0 & 0 & 0 & 0 & 0 \\ 0 & 0 & 0 & 0 & 0 & 0 \\ 0 & 0 & 0 & 0 & 0 & N_{i,y} \\ 0 & 0 & 0 & 0 & 0 & N_{i,x} \\ 0 & 0 & 0 & 0 & 0 & 0 \end{bmatrix}$$

The stress is related to stress parameters $\boldsymbol{\beta}$ via the stress interpolation function φ

$$\boldsymbol{\sigma} = \varphi\boldsymbol{\beta} \tag{10}$$

where

$$\begin{aligned} \varphi &= \begin{bmatrix} \varphi_{x0} & \bar{z}^2\varphi_{x1} & 0 & 0 \\ \varphi_{y0} & \bar{z}^2\varphi_{y1} & 0 & 0 \\ \varphi_{xy0} & \bar{z}^2\varphi_{xy1} & 0 & 0 \\ 0 & 0 & (\bar{z} - \bar{z}^3)\varphi_{yz0} & (\bar{z}^3 - \bar{z}^5)\varphi_{yz1} \\ 0 & 0 & (\bar{z} - \bar{z}^3)\varphi_{zx0} & (\bar{z}^3 - \bar{z}^5)\varphi_{zx1} \\ 0 & 0 & (1 - \bar{z}^2)\varphi_{z0} & (\bar{z}^2 - \bar{z}^4)\varphi_{z1} \end{bmatrix} \\ &= \begin{bmatrix} \varphi_0 & \bar{z}^2\varphi_1 & (\bar{z} - \bar{z}^3)\varphi_2 + (1 - \bar{z}^2)\varphi_3 & (\bar{z}^3 - \bar{z}^5)\varphi_4 + (\bar{z}^2 - \bar{z}^4)\varphi_5 \end{bmatrix} \end{aligned} \tag{11}$$

and

$$\varphi_0 = \begin{bmatrix} \varphi_{x0} \\ \varphi_{y0} \\ \varphi_{xy0} \\ 0 \\ 0 \\ 0 \end{bmatrix}, \quad \varphi_1 = \begin{bmatrix} \varphi_{x1} \\ \varphi_{y1} \\ \varphi_{xy1} \\ 0 \\ 0 \\ 0 \end{bmatrix}, \quad \varphi_2 = \begin{bmatrix} 0 \\ 0 \\ 0 \\ \varphi_{yz0} \\ \varphi_{zx0} \\ 0 \end{bmatrix}, \quad \varphi_3 = \begin{bmatrix} 0 \\ 0 \\ 0 \\ 0 \\ 0 \\ \varphi_{z0} \end{bmatrix}, \quad \varphi_4 = \begin{bmatrix} 0 \\ 0 \\ 0 \\ \varphi_{yz1} \\ \varphi_{zx1} \\ 0 \end{bmatrix}, \quad \varphi_5 = \begin{bmatrix} 0 \\ 0 \\ 0 \\ 0 \\ 0 \\ \varphi_{z1} \end{bmatrix}$$

The stress parameters

$$\boldsymbol{\beta}^{\mathrm{T}} = [\,\boldsymbol{\beta}_0^{\mathrm{T}} \quad \boldsymbol{\beta}_1^{\mathrm{T}} \quad \boldsymbol{\beta}_{23}^{\mathrm{T}} \quad \boldsymbol{\beta}_{45}^{\mathrm{T}}\,]$$

The dimensions of vectors $\boldsymbol{\beta}_0$, $\boldsymbol{\beta}_1$, $\boldsymbol{\beta}_{23}$, and $\boldsymbol{\beta}_{45}$ are identical to the columns of φ_0, φ_1, φ_2 (or φ_3) and φ_4 (or φ_5), respectively. The actual dimensions of vectors φ and $\boldsymbol{\beta}$ (or more specifically $\boldsymbol{\beta}_0$, $\boldsymbol{\beta}_1$, $\boldsymbol{\beta}_{23}$, and $\boldsymbol{\beta}_{45}$) are dependent on the assumed stress field used in the element formulation. An example element will be detailed in Section 6 and the corresponding dimensions of vectors $\boldsymbol{\beta}_0$, $\boldsymbol{\beta}_1$, $\boldsymbol{\beta}_{23}$, and $\boldsymbol{\beta}_{45}$ will be provided.

Substituting Eqs. (5), (8) and (10) into the functional in Eq. (4), and making use of the stationary condition, gives

$$\boldsymbol{\beta} = \mathbf{H}^{-1}\mathbf{G}\mathbf{q} \tag{12}$$

and the discretized equations of equilibrium of element "e"

$$\mathbf{K}^{(e)}\mathbf{q} = \bar{\mathbf{f}}^{(e)} \tag{13}$$

where the stiffness matrix of element 'e' is

$$\mathbf{K}^{(e)} = \mathbf{G}^{\mathrm{T}}\mathbf{H}^{-1}\mathbf{G} \tag{14}$$

and the load vector

$$\bar{\mathbf{f}} = \int_{-h}^{h} \left\{ \iint_{A^{(e)}} \mathbf{N}^{\mathrm{T}}\bar{\mathbf{f}}\,\mathrm{d}A + \int_{S_\sigma^{(e)}} \mathbf{N}^{\mathrm{T}}\bar{\mathbf{T}}\,\mathrm{d}s \right\} \mathrm{d}z \tag{15}$$

The characteristic matrices of the element are

$$\mathbf{H} = \int_{-h}^{h} \int_{A^{(e)}} \boldsymbol{\varphi}^{\mathrm{T}}\mathbf{S}\boldsymbol{\varphi}\,\mathrm{d}A\,\mathrm{d}z, \quad \mathbf{G} = \int_{-h}^{h} \int_{A^{(e)}} \boldsymbol{\varphi}^{\mathrm{T}}\mathbf{B}\,\mathrm{d}A\,\mathrm{d}z \tag{16}$$

As the functions are relatively easily integrable, we have integrated the matrices in Eq. (16) analytically in the z-direction ('thickness' direction). However, in the xy-plane, the integration was performed using the traditional numerical Gauss integration rule. The integrals along the z-direction are given in the following

$$\int_{-h}^{h} \boldsymbol{\varphi}^{\mathrm{T}}\mathbf{S}\boldsymbol{\varphi}\,\mathrm{d}z = 2h \begin{bmatrix} \varphi_0^{\mathrm{T}}\mathbf{S}\varphi_0 & \frac{1}{3}\varphi_0^{\mathrm{T}}\mathbf{S}\varphi_1 & \frac{2}{3}\varphi_0^{\mathrm{T}}\mathbf{S}\varphi_3 & \frac{2}{15}\varphi_0^{\mathrm{T}}\mathbf{S}\varphi_5 \\ & \frac{1}{5}\varphi_1^{\mathrm{T}}\mathbf{S}\varphi_1 & \frac{2}{15}\varphi_1^{\mathrm{T}}\mathbf{S}\varphi_3 & \frac{2}{35}\varphi_1^{\mathrm{T}}\mathbf{S}\varphi_5 \\ & & \frac{8}{105}\varphi_2^{\mathrm{T}}\mathbf{S}\varphi_2 + \frac{8}{15}\varphi_3^{\mathrm{T}}\mathbf{S}\varphi_3 & \frac{8}{315}\varphi_2^{\mathrm{T}}\mathbf{S}\varphi_4 + \frac{8}{105}\varphi_3^{\mathrm{T}}\mathbf{S}\varphi_5 \\ \text{sym} & & & \frac{8}{693}\varphi_4^{\mathrm{T}}\mathbf{S}\varphi_4 + \frac{8}{315}\varphi_5^{\mathrm{T}}\mathbf{S}\varphi_5 \end{bmatrix}$$

$$\int_{-h}^{h} \boldsymbol{\varphi}^{\mathrm{T}}\mathbf{B}^{(i)}\,\mathrm{d}z = 2h \begin{bmatrix} \varphi_0^{\mathrm{T}}\mathbf{B}_0^{(i)} + \frac{h^2}{3}\varphi_0^{\mathrm{T}}\mathbf{B}_2^{(i)} \\ \frac{1}{3}\varphi_1^{\mathrm{T}}\mathbf{B}_0^{(i)} + \frac{h^2}{5}\varphi_1^{\mathrm{T}}\mathbf{B}_2^{(i)} \\ \frac{2}{3}\varphi_3^{\mathrm{T}}\mathbf{B}_0^{(i)} + \frac{2h}{15}\varphi_2^{\mathrm{T}}\mathbf{B}_1^{(i)} + \frac{2h^2}{15}\varphi_3^{\mathrm{T}}\mathbf{B}_2^{(i)} + \frac{2h^3}{35}\varphi_2^{\mathrm{T}}\mathbf{B}_3^{(i)} \\ \frac{2}{15}\varphi_5^{\mathrm{T}}\mathbf{B}_0^{(i)} + \frac{2h}{35}\varphi_4^{\mathrm{T}}\mathbf{B}_1^{(i)} + \frac{2h^2}{35}\varphi_5^{\mathrm{T}}\mathbf{B}_2^{(i)} + \frac{2h^3}{63}\varphi_4^{\mathrm{T}}\mathbf{B}_3^{(i)} \end{bmatrix} \tag{17}$$

As defined by Wu and Bufler (1991), Eq. (13) could not be solved uniquely unless the displacement and stress parameters are selected appropriately so that they satisfy the condition given in Eq. (18)

$$n_\beta \geqslant n_q - n_r \tag{18}$$

where n_β and n_q represent the number of element stress parameters $\boldsymbol{\beta}$ and nodal displacement parameters $\mathbf{q}$, respectively, and n_r ($=3$) is the number of independent rigid body motions which is three in this case.

4. Optimisation of element trial stresses

In the formulation of the solid hybrid stress element, the performance, or the capability of the element in predicting stresses can be improved through the introduction of incompatible displacements (Pian and Wu, 1988; Wu and Bufler, 1991; Wu and Cheung, 1995). Let us add an incompatible displacement field each (as shown in Eq. (19)) to the compatible displacement field in Eq. (1).

$$u_\lambda(x, y, z) = u_{0\lambda}(x, y) + z^2 u_{1\lambda}(x, y)$$
$$v_\lambda(x, y, z) = v_{0\lambda}(x, y) + z^2 v_{1\lambda}(x, y) \tag{19}$$
$$w_\lambda(x, y, z) = z w_{0\lambda}(x, y) + z^3 w_{1\lambda}(x, y)$$

Then let us substitute the resulting field into Eq. (4). The stationary condition of the functional provides equilibrium, compatibility, equilibrium of traction between elements and the prescribed traction constraints if and only if the integral shown in Eq. (20) vanishes.

$$\int_{-h}^{h} \oint_{\partial A^{(e)}} \boldsymbol{\sigma}^{\mathrm{T}} \mathbf{n}^{\mathrm{T}} \delta \mathbf{u}_\lambda \, \mathrm{d}s \, \mathrm{d}z = 0 \tag{20}$$

in which $\partial A^{(e)}$ is the boundary of the element, and $\mathbf{n}$ is the matrix of direction cosines of the unit outward normal to the element boundary

$$\mathbf{n} = \begin{bmatrix} n_1 & 0 & n_2 & 0 & n_3 & 0 \\ 0 & n_2 & n_1 & n_3 & 0 & 0 \\ 0 & 0 & 0 & n_2 & n_1 & n_3 \end{bmatrix}$$

In this derivation we have used the traction free state on the lateral surfaces. Since inner incompatible displacements $\mathbf{u}_\lambda$ can be selected arbitrarily, Eq. (20) can be rewritten as

$$\int_{-h}^{h} \oint_{\partial A^{(e)}} \boldsymbol{\sigma}^{\mathrm{T}} \mathbf{n}^{\mathrm{T}} \mathbf{u}_\lambda \, \mathrm{d}s \, \mathrm{d}z = 0 \tag{21}$$

By integrating Eq. (21) along the thickness, we obtain

$$\oint_{\partial A^{(e)}} \left\{ \left[\left(\sigma_{x0} + \frac{1}{3} \sigma_{x1} \right) n_1 + \left(\tau_{xy0} + \frac{1}{3} \tau_{xy1} \right) n_2 \right] u_{0\lambda} + h^2 \left[\left(\frac{1}{3} \sigma_{x0} + \frac{1}{5} \sigma_{x1} \right) n_1 + \left(\frac{1}{3} \tau_{xy0} + \frac{1}{5} \tau_{xy1} \right) n_2 \right] u_{1\lambda} \right.$$
$$+ \left[\left(\tau_{xy0} + \frac{1}{3} \tau_{xy1} \right) n_1 + \left(\sigma_{y0} + \frac{1}{3} \sigma_{y1} \right) n_2 \right] v_{0\lambda} + h^2 \left[\left(\frac{1}{3} \tau_{xy0} + \frac{1}{5} \tau_{xy1} \right) n_1 + \left(\frac{1}{3} \sigma_{y0} + \frac{1}{5} \sigma_{y1} \right) n_2 \right] v_{1\lambda}$$
$$+ h \left[\left(\frac{2}{15} \tau_{zx0} + \frac{2}{35} \tau_{zx1} \right) n_1 + \left(\frac{2}{15} \tau_{yz0} + \frac{2}{35} \tau_{yz1} \right) n_2 \right] w_{0\lambda}$$
$$+ \left. h^3 \left[\left(\frac{2}{35} \tau_{zx0} + \frac{2}{63} \tau_{zx1} \right) n_1 + \left(\frac{2}{35} \tau_{yz0} + \frac{2}{63} \tau_{yz1} \right) n_2 \right] w_{1\lambda} \right\} \mathrm{d}s = 0$$

In order to meet the constraint above, we let the in-plane fields as follows:

$$\oint_{\partial A^{(e)}} (\sigma_{x0} n_1 + \tau_{xy0} n_2) u_{0\lambda} \, \mathrm{d}s = 0, \qquad \oint_{\partial A^{(e)}} (\sigma_{x1} n_1 + \tau_{xy1} n_2) u_{0\lambda} \, \mathrm{d}s = 0$$

$$\oint_{\partial A^{(e)}} (\tau_{xy0} n_1 + \sigma_{y0} n_2) v_{0\lambda} \, \mathrm{d}s = 0, \qquad \oint_{\partial A^{(e)}} (\tau_{xy1} n_1 + \sigma_{y1} n_2) v_{0\lambda} \, \mathrm{d}s = 0$$

$$\oint_{\partial A^{(e)}} (\sigma_{x0} n_1 + \tau_{xy0} n_2) u_{1\lambda} \, \mathrm{d}s = 0, \qquad \oint_{\partial A^{(e)}} (\sigma_{x1} n_1 + \tau_{xy1} n_2) u_{1\lambda} \, \mathrm{d}s = 0$$

$$\oint_{\partial A^{(e)}} (\tau_{xy0} n_1 + \sigma_{y0} n_2) v_{1\lambda} \, \mathrm{d}s = 0, \qquad \oint_{\partial A^{(e)}} (\tau_{xy1} n_1 + \sigma_{y1} n_2) v_{1\lambda} \, \mathrm{d}s = 0$$

and the out-of-plane fields as follows:

$$\oint_{\partial A^{(e)}} (\tau_{zx0} n_1 + \tau_{yz0} n_2) w_{0\lambda} \, \mathrm{d}s = 0, \qquad \oint_{\partial A^{(e)}} (\tau_{zx1} n_1 + \tau_{yz1} n_2) w_{0\lambda} \, \mathrm{d}s = 0$$

$$\oint_{\partial A^{(e)}} (\tau_{zx0} n_1 + \tau_{yz0} n_2) w_{1\lambda} \, \mathrm{d}s = 0, \qquad \oint_{\partial A^{(e)}} (\tau_{zx1} n_1 + \tau_{yz1} n_2) w_{1\lambda} \, \mathrm{d}s = 0$$

A convenient way to meet the constraints above is using the same interpolation functions in the interpolation of the first and the second terms subscripted with "0" and "1" in all the displacement and stress

component functions. In other words, the interpolation functions used for u_0, v_0, w_0, σ_{x0}, σ_{y0}, τ_{xy0}, τ_{yz0} and τ_{zx0} are the same as that for u_1, v_1, w_1, σ_{x1}, σ_{y1}, τ_{xy1}, τ_{yz1} and τ_{zx1}, respectively. This further simplifies that only the following three equations are required to be considered:

$$\oint_{\partial A^{(e)}} (\sigma_{x0} n_1 + \tau_{xy0} n_2) u_{0\lambda}\, \mathrm{d}s = 0$$

$$\oint_{\partial A^{(e)}} (\tau_{xy0} n_1 + \sigma_{y0} n_2) v_{0\lambda}\, \mathrm{d}s = 0 \tag{22}$$

$$\oint_{\partial A^{(e)}} (\tau_{zx0} n_1 + \tau_{yz0} n_2) w_{0\lambda}\, \mathrm{d}s = 0$$

The first two equations in (22) are those equations for the plane components given in Pian and Wu (1988) and Wu and Bufler (1991), while the last one is the same as that of the St. Venant torsion problem discussed by Xiao et al. (1999). In order to satisfy Eq. (22) in the element formulation, we further divide the relevant first terms of the stress components in Eq. (3) into constant terms and high-order terms as shown in Eq. (23).

$$\sigma_{x0} = \sigma_{x0c} + \sigma_{x0h}$$

$$\sigma_{y0} = \sigma_{y0c} + \sigma_{y0h}$$

$$\sigma_{xy0} = \sigma_{xy0c} + \sigma_{xy0h}$$

$$\sigma_{z0} = \sigma_{z0c} + \sigma_{z0h} \tag{23}$$

$$\sigma_{yz0} = \sigma_{yz0c} + \sigma_{yz0h}$$

$$\sigma_{zx0} = \sigma_{zx0c} + \sigma_{zx0h}$$

We then obtain from Eq. (22) the patch test conditions (PTC) as shown in Eq. (24) for evaluating the incompatible displacement fields that pass the PTC,

$$\oint_{\partial A^{(e)}} (\sigma_{x0c} n_1 + \tau_{xy0c} n_2) u_{0\lambda}\, \mathrm{d}s = 0$$

$$\oint_{\partial A^{(e)}} (\tau_{xy0c} n_1 + \sigma_{y0c} n_2) v_{0\lambda}\, \mathrm{d}s = 0 \tag{24}$$

$$\oint_{\partial A^{(e)}} (\tau_{zx0c} n_1 + \tau_{yz0c} n_2) w_{0\lambda}\, \mathrm{d}s = 0$$

and the stress optimisation conditions (OPC) as shown in Eq. (25) for optimising the trial stresses, as discussed by Pian and Wu (1988), Wu and Bufler (1991), and Wu and Cheung (1995)

$$\oint_{\partial A^{(e)}} (\sigma_{x0h} n_1 + \tau_{xy0h} n_2) u_{0\lambda}\, \mathrm{d}s = 0$$

$$\oint_{\partial A^{(e)}} (\tau_{xy0h} n_1 + \sigma_{y0h} n_2) v_{0\lambda}\, \mathrm{d}s = 0 \tag{25}$$

$$\oint_{\partial A^{(e)}} (\tau_{zx0h} n_1 + \tau_{yz0h} n_2) w_{0\lambda}\, \mathrm{d}s = 0$$

For the hybrid stress element formulated from the Hellinger–Reissner principle, it has been proved by Wu and Bufler (1991) and Wu and Pian (1997) that the PTC (24) is equivalent to the stability condition popularly known as the Babuska–Brezzi (BB) condition. The hybrid stress element presented in this paper is, therefore, considered to have satisfied the stability condition.

5. 3D displacement and stress fields for in-plane actions of a hollow solid

Consider a hollow solid shown in Fig. 2. The 3D displacement field of this hollow solid is considered the same as for the solid given in Eq. (1). The stress fields were, however assumed as in Eq. (26) to account for the additional traction free planes.
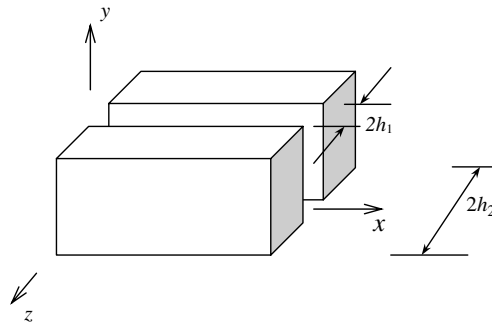
Fig. 2. A symmetric hollow solid.

$$\sigma_x(x,y,z) = \sigma_{x0}(x,y) + z^2\sigma_{x1}(x,y)$$
$$\sigma_y(x,y,z) = \sigma_{y0}(x,y) + z^2\sigma_{y1}(x,y)$$
$$\tau_{xy}(x,y,z) = \tau_{xy0}(x,y) + z^2\tau_{xy1}(x,y)$$
$$\tau_{yz}(x,y,z) = zf(z)\tau_{yz0}(x,y) + z^3f(z)\tau_{yz1}(x,y) \tag{26}$$
$$\tau_{zx}(x,y,z) = zf(z)\tau_{zx0}(x,y) + z^3f(z)\tau_{zx1}(x,y)$$
$$\sigma_z(x,y,z) = f(z)\sigma_{z0}(x,y) + z^2f(z)\sigma_{z1}(x,y)$$

where

$$f(z) = (h_1^2 - z^2)(h_2^2 - z^2) \tag{27}$$

and h_1 and h_2 are half thickness of the inner hole and the body, respectively, as shown in Fig. 2. These functions are different to that used for the solid element in (3) as the solid element possesses only two external traction free surfaces unlike the bodies with holes.

The procedure similar to that presented in Sections 3 of this paper was followed to deduce the characteristic matrices **H** and **G** for the hollow element. The trial stresses were also optimised for the hollow element as per details presented in Section 4 of this paper. Details of this hollow element formulation can be found in Dhanasekar and Xiao (2001).

6. Four-noded hybrid stress elements for solid and hollow element formulations

With reference to the four-noded isoparametric element, the shape functions employed in Eq. (7) are the widely used bilinear interpolation functions

$$N_i = \frac{1}{4}(1 + \xi_i\xi)(1 + \eta_i\eta) \tag{28}$$

where (ξ, η) represent the isoparametric coordinates, (ξ_i, η_i) represent the isoparametric coordinates of point i with the global coordinates (x_i, y_i), $i = 1, 2, 3, 4$.

Since the PTC and OPC for plane components in Eqs. (24) and (25) are the same as the traditional plane problems, the optimised trial stresses of a plane hybrid stress element P-S introduced by Pian and Sumihara (1984) and Pian and Wu (1988) are adopted here directly. We thus have

$$\begin{bmatrix} \varphi_{x0} \\ \varphi_{y0} \\ \varphi_{xy0} \end{bmatrix} = \begin{bmatrix} \varphi_{x1} \\ \varphi_{y1} \\ \varphi_{xy1} \end{bmatrix} = \begin{bmatrix} 1 & 0 & 0 & a_1^2\eta & a_3^2\xi \\ 0 & 1 & 0 & b_1^2\eta & b_3^2\xi \\ 0 & 0 & 1 & a_1b_1\eta & a_3b_3\xi \end{bmatrix} \tag{29}$$

where coefficients a_i and b_i ($i = 1, 2, 3$) are dependent on the element nodal coordinates as follows:

$$\begin{bmatrix} a_1 & b_1 \\ a_2 & b_2 \\ a_3 & b_3 \end{bmatrix} = \frac{1}{4} \begin{bmatrix} -1 & 1 & 1 & -1 \\ 1 & -1 & 1 & -1 \\ -1 & -1 & 1 & 1 \end{bmatrix} \begin{bmatrix} x_1 & y_1 \\ x_2 & y_2 \\ x_3 & y_3 \\ x_4 & y_4 \end{bmatrix} \tag{30}$$

The procedure discussed by Xiao et al. (1999) was adopted to optimise the out-of-plane shear stresses even though the optimised trial stresses were inappropriate here. This is because constant stress state must be retained in the current case unlike the St. Venant torsion problem discussed in Xiao et al. (1999). Therefore, the primary assumed stresses take the form

$$\left\{ \begin{matrix} \tau_{yz0} \\ \tau_{zx0} \end{matrix} \right\} = \begin{bmatrix} 1 & 0 & \xi & 0 & \eta & 0 \\ 0 & 1 & 0 & \eta & 0 & \xi \end{bmatrix}, \quad \beta = \left\{ \begin{matrix} \tau_{yz0c} \\ \tau_{zx0c} \end{matrix} \right\} + \left\{ \begin{matrix} \tau_{yz0h} \\ \tau_{zx0h} \end{matrix} \right\} \tag{31}$$

where

$$\left\{ \begin{matrix} \tau_{yz0c} \\ \tau_{zx0c} \end{matrix} \right\} = \begin{bmatrix} 1 & 0 \\ 0 & 1 \end{bmatrix}, \quad \beta_c \left\{ \begin{matrix} \tau_{yz0h} \\ \tau_{zx0h} \end{matrix} \right\} = \begin{bmatrix} \xi & 0 & \eta & 0 \\ 0 & \eta & 0 & \xi \end{bmatrix} \beta_h$$

The incompatible term employed here is

$$w_{0\lambda} = \begin{bmatrix} 1 - \xi^2 & 1 - \eta^2 \end{bmatrix} \lambda \tag{32}$$

Substituting (31) and (32) into the last equation in (25), we obtain the optimised interpolation functions for out-of-plane trial stresses as shown in Eq. (33)

$$\begin{bmatrix} \varphi_{yz0} \\ \varphi_{zx0} \\ \varphi_{z0} \end{bmatrix} = \begin{bmatrix} \varphi_{yz1} \\ \varphi_{zx1} \\ \varphi_{z1} \end{bmatrix} = \begin{bmatrix} 1 & 0 & b_1\eta & b_3\xi & 0 & 0 & 0 \\ 0 & 1 & a_1\eta & a_3\xi & 0 & 0 & 0 \\ 0 & 0 & 0 & 0 & 1 & \xi & \eta \end{bmatrix} \tag{33}$$

In the element formulation discussed in Section 3, we now use the assumed displacement given in Eq. (5), in which N_i is defined by Eq. (28), and the trial stresses given in Eq. (10), in which Eqs. (29) and (33) are used as stress interpolation functions of the plane and out-plane components, respectively; correspondingly the dimensions of $\text{DIM}(\beta_0) = \text{DIM}(\beta_1) = 5$; and $\text{DIM}(\beta_{23}) = \text{DIM}(\beta_{45}) = 7$. The resulting element has 24 stress parameters β and is therefore designated as Q3D24β for solid element and Q3D24βH for hollow element. For theses elements, $n_\beta = 24$, $n_q = 24$, and hence they meet the stability condition of Eq. (18).

Second order Gauss quadrature is employed for the element formulation. Theoretical analysis and results of eigenvalue checks show that the element is rank-sufficient.

7. Numerical tests

In this section, we first study the pattern of the convergence with *h*-refinement as well as the sensitivity to aspect ratio of the Q3D24β element. Then using this element we will examine the effect of the thickness of the solids on the displacement and stress fields. Test results for the Q3D24βH element can be found in Dhanasekar and Xiao (2001).

7.1. Convergence with h-refinement

A classical 2D flexural beam problem with span to depth ratio 5.0 subjected to pure bending was used to examine the convergence with *h*-refinement. The span, depth, and thickness of the beam were considered as 10, 2 and 2 (unit free measurements), respectively. As this example is widely used as the bench marking problem for classical plane stress elements, the current Q3D24β element have also been validated through this problem. The loading and material properties for the beam problem were chosen in such a way that the theoretical vertical deflection of the cantilever beam at its tip would be 100 and the top fibre stress σ_x be –3000. The Young's

modulus used in the problem was 1500 and the Poisson's ratio was kept as 0.25. The free end of the beam was subjected to a positive bending moment of 2000 per unit thickness with its unit consistent with that of the Young's modulus.

The convergence with h-refinement was studied by meshing the beams with 3, 5 and 20 elements as shown in Fig. 3(a)–(c), respectively. u_0, u_1, v_0 and v_1 of the node $(0,0)$ and u_0, u_1 of the node $(0,2)$ are fixed.

The results of the analysis for h-refinement are plotted in Fig. 4 for the convergence of stress σ_x at $(1,2)$ and tip deflection. Rapid convergence is obtained even when the beam was modelled with only five elements.

7.2. Sensitivity to element aspect ratio

In meshing complex problems (for example mortar joints in masonry structures) engineers confront with the problem of aspect ratio of elements. In order to test the sensitivity of the aspect ratio of the current elements, the cantilever problem reported in the previous section was used. The mesh used in the analysis is shown in Fig. 5.

Four aspect ratios namely, 5, 10, 20 and 100 were used. The aspect ratio 100 was achieved from a non-uniform meshing of the problem and all other aspect ratios were achieved from uniform meshing. The results of the study presented in Fig. 6 show clearly that the current Q3D24β element is not sensitive to aspect ratio. The regularity of mesh without large distortion, rather than the narrow aspect ratio is important in achieving good results with the current Q3D24β element.
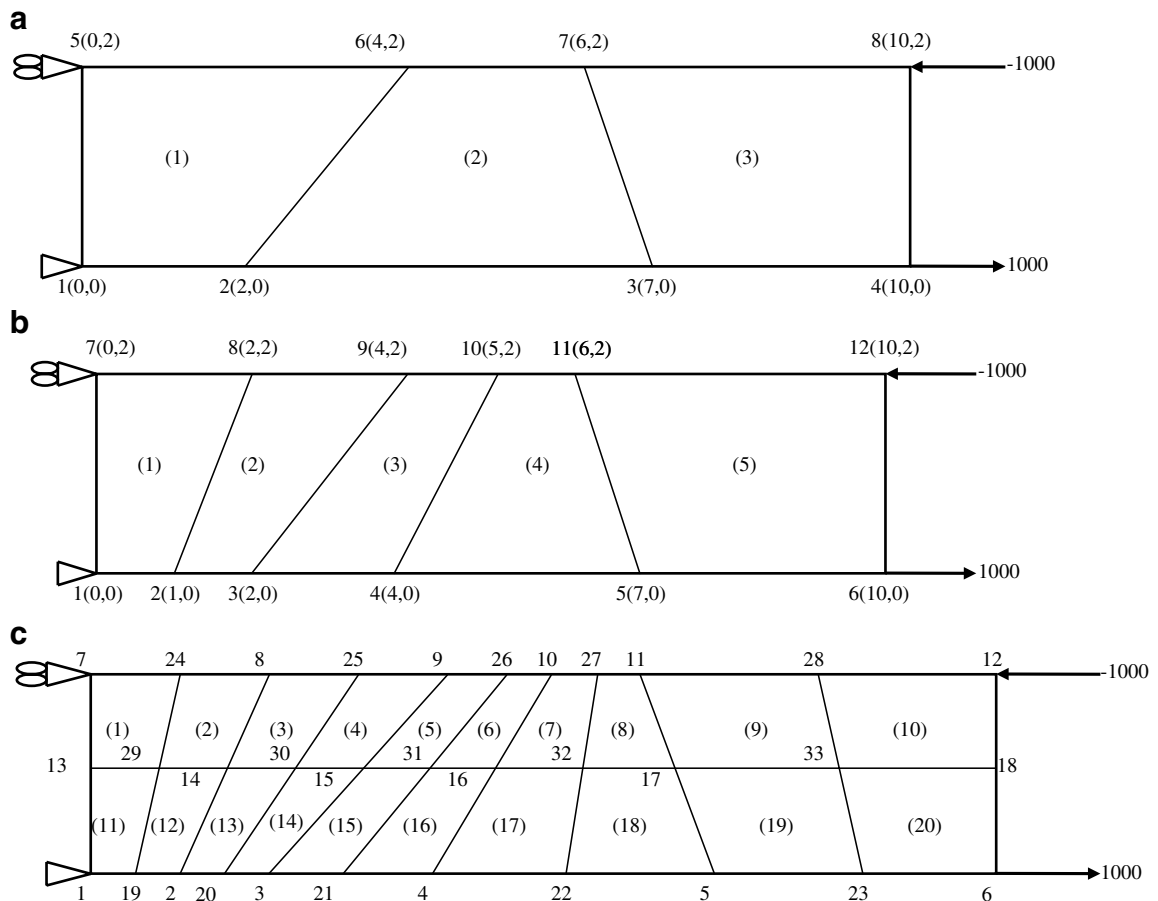

Fig. 3. Cantilever beam for h-refinement test. Mesh with (a) three elements, (b) five elements, (c) twenty elements.
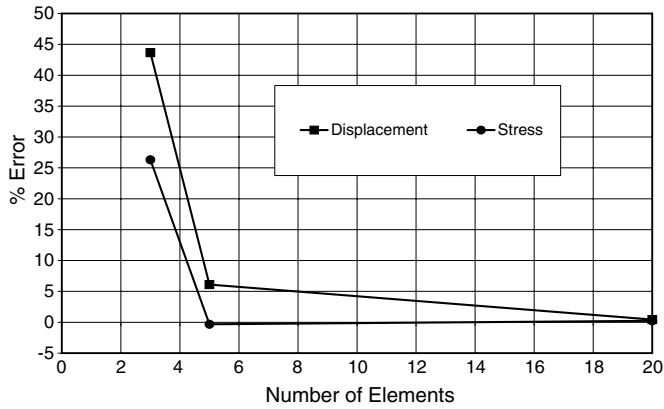
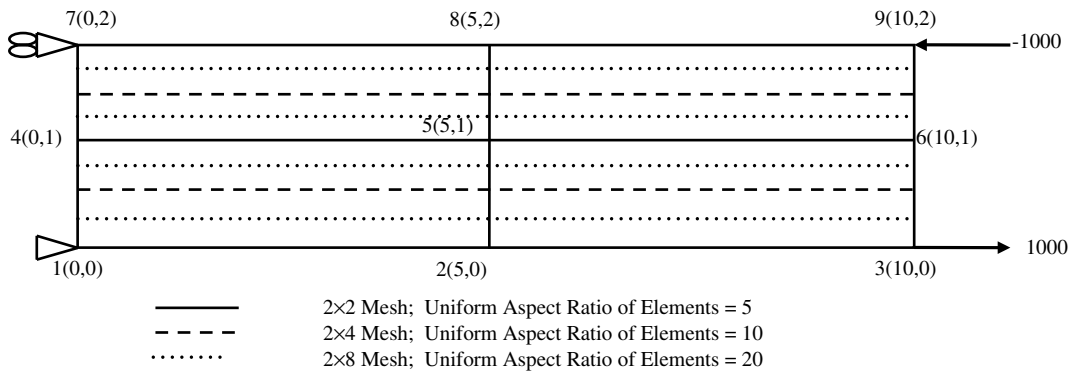Fig. 4. Convergence of stress and displacement with *h*-refinement.

2×2 Mesh; Uniform Aspect Ratio of Elements = 5
2×4 Mesh; Uniform Aspect Ratio of Elements = 10
2×8 Mesh; Uniform Aspect Ratio of Elements = 20

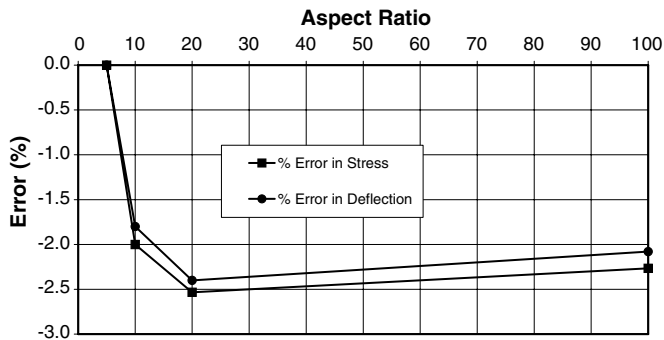Fig. 5. Mesh of cantilever beam for aspect ratio test.

Fig. 6. Sensitivity of stress and displacement to aspect ratio of element.

7.3. Effect of thickness

The current elements were used to examine the effect of the thickness of the solid on the stress and displacement fields. A cantilever beam used by Ye (1997) was used for this purpose as shown in Fig. 7. A concrete cantilever beam of span 2000 mm, depth 200 mm and varying thickness 100 mm, 200 mm, 1000 mm, 2000 mm, 4000 mm, 10,000 mm and 20,000 mm was considered. A total load of −10,000 N distributed
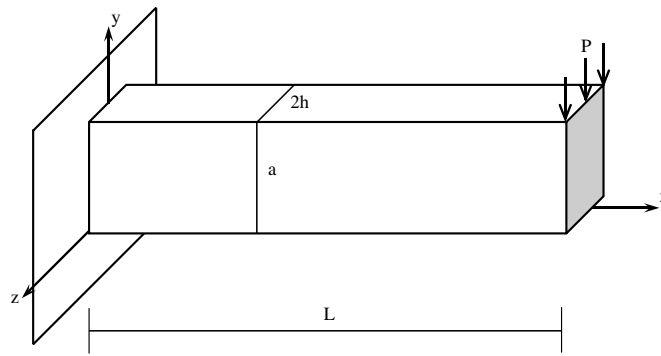
Fig. 7. Concrete cantilever beam for studying the effect of thickness.

uniformly along the thickness direction was applied at the tip of the cantilever. The modulus of elasticity was kept as 20 GPa and the Poisson's ratio was chosen as 0.15.

Regular mesh with 128 elements (16 elements along the length and 8 elements in the depth direction) was used in the 2D analysis using the current Q3D24β element. The node $(0,0)$ that represented the centroid of the fixed end was fixed in both x-(u_0, u_1) and y-(v_0, v_1) directions; other nodes $(0, y, 0)$ on the left-hand side were fixed only in the x-direction (u_0, u_1). The beams of varying thickness were also modelled in ABAQUS using an eight noded linear brick element (C3D8). The number of elements for the thinnest beam (100 mm) was 576 ($16 \times 6 \times 6$) and the thickest beam (20,000 mm) was 2400 ($16 \times 6 \times 25$).

The thickness to depth ratio varied from 0.5 to 100. Deflection at the neutral axis level on the tip (200 mm, 100 mm, 0 mm) and stresses at a point (62.5 mm, 187.5 mm, 0 mm) were monitored. As the total load was kept constant, with the increase in thickness the σ_x stress and v deflection reduced markedly as shown in Table 1. The dominant axial normal stress σ_x predicted by the current Q3D24β element is in very good agreement with the 3D ABAQUS analysis result (maximum error of 3.2%) for the range of thickness to depth ratio of 0.5–100.

The deflection predicted by the Q3D24β element is also in very good agreement with the 3D ABAQUS analysis (maximum error 0.6%). Also shown in the table are the vertical deflections (v) predicted by the analytical expression (34) assuming plane stress and plane strain conditions (Ugural and Fenster, 1995)

$$v = \frac{PL^3}{3EI} + \frac{Ph^2(1+v)L}{EI} \tag{34}$$

where P is the total load, L is the span, I is the moment of inertia of the section and E and v are the Young's modulus and Poisson's ratio, respectively.

For the plane stress condition, the E and v were used as the assumed values of 20GPa and 0.15, respectively. For the plane strain condition E was replaced by $\frac{E}{(1-v^2)}$ and v was replaced by $\frac{v}{(1-v)}$.

It could be seen that the deflection predicted by the Q3D24β element (and ABAQUS 3D analysis) is close to the plane stress calculation for $\left(\frac{h}{a}\right) < 1.0$ and close to plane strain calculation for $\left(\frac{h}{a}\right) \geqslant 10$ where h and a are

Table 1
Effect of thickness of the cantilever beam on its stress and deformation

(h/a)	σ_x (62.5, 187.5, 0.0) (MPa)			δ (2000, 100, 0) (mm)					σ_z (62.5, 187.5, 0.0) (MPa)		
	Current El	ABAQ_3D	% Difference	Current El	ABAQ_3D	% Difference	Pl stress	Pl strain	Current El	ABAQ_3D	% Difference
0.5	12.771	12.737	0.27	−10.060	−10.040	0.20	−10.086	–	–	–	–
1	6.435	6.380	0.85	−5.024	−5.020	0.08	−5.043	–	–	–	–
5	1.359	1.316	3.19	−0.996	−0.997	−0.09	−1.009	−0.986	0.189	0.196	3.42
10	0.671	0.667	0.60	−0.498	−0.495	0.62	−0.504	−0.493	0.092	0.097	5.36
20	0.327	0.318	2.86	−0.248	−0.247	0.48	−0.252	−0.247	0.044	0.048	8.18
50	0.128	0.127	1.14	−0.099	−0.098	0.26	–	−0.099	0.017	0.019	9.32
100	0.064	0.063	0.99	−0.049	−0.049	0.06	–	−0.049	0.008	0.010	11.44

dimensions shown in Fig. 7. It could be seen for $1 \leqslant \frac{h}{a} \leqslant 10$, the deflection is in between the plane stress and plane strain solutions, with the increase in the ratio moving closer to plane strain. From this result, it may be concluded that the Q3D24β element can analyse solids and structures irrespective of their thickness. For solids whose $1 \leqslant \frac{h}{a} \leqslant 10$, normally neither plane stress nor plane strain solution will be applicable; only a 3D solution must be sought. However the Q3D24β element presented in this paper have the potential to solve such problems.

As the Q3D24β element predicts the σ_z stress, its prediction was also compared with that of the ABAQUS 3D solution. The results compare generally very well. At very low stress values a maximum error of 11.4% was reported. In the region of $1 \leqslant \frac{h}{a} \leqslant 10$, the error was only 5.4%.

8. Application of the current elements

In this section, we present a comparative study using the present Q3D24β and Q3D24βH elements and a 3D incompatible element (C3D8I) available in ABAQUS by carrying out the analysis of a cube shaped cantilevered solid subjected to lateral loading and a hollow masonry prism subjected to vertical compression.

8.1. Cube shaped solid cantilever

As the element is formulated using 3D semi-analytical and hybrid stress approach, it was decided to validate all fields predicted by the element by comparing them with the prediction of the C3D8I element available in ABAQUS.

We considered a cube shaped elastic solid of dimension $2 \times 2 \times 2$ shown in Fig. 8 as the example problem for validation. The Young's modulus and the Poisson's ratio of the solid were kept as 1500 and 0.25, respectively.

The origin of the coordinate system was chosen at the lower left edge of the middle plane of the cube. The xy-plane defined the middle section of the cube and z-axis defined its thickness direction (from -1 to $+1$). The left yz-plane was fixed and the vertical load was applied at the top edge of the right yz-plane in the $-y$-direction. The vertical load was 1000 per unit length with its unit consistent with that of the Young's modulus.

Due to symmetry about the xy-plane, only half of the solid was analysed using the 3D element in ABAQUS. A $10 \times 10 \times 16$ mesh with 1600 brick elements and 2057 nodes was used in the 3D analysis. The displacement and stress components were monitored at the centre of the solid ($x = 1.0$, $y = 1.0$, $z = 0$–1.0). The trace
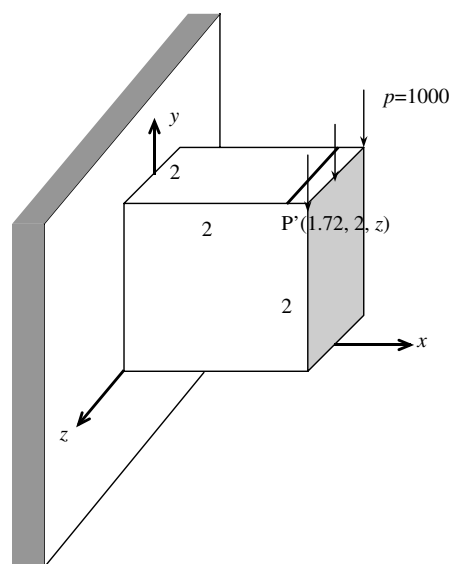

Fig. 8. A cube problem.

of the intersection between the top horizontal surface of the solid ($y = 2.0$) and a vertical plane ($x = 1.72$) as shown in Fig. 8 was used for validating σ_z as it was the largest in this region.

The same problem was then modelled using the Q3D24β element. The node $(0,0)$ was fixed in both x-(u_0, u_1) and y-(v_0, v_1) directions; other nodes $(0, y, 0)$ on the left-hand side were fixed only in the x-direction (u_0, u_1). Only the middle section was required to be meshed in this case and a 8×8 mesh was used. The displacement and stress were monitored at a point P ($x = 1.0$, $y = 1.0$) and P' ($x = 1.72$ $y = 2.0$). The variation of displacement and stress components through the thickness was then determined from Eqs. (1) and (3), respectively. Comparison of the results predicted by the two methods is presented in Fig. 9 for stresses and 10 for displacements.

It could be seen from the graphs shown in Figs. 9 and 10 that the prediction of the stresses and displacements by the Q3D24β element is in reasonable agreement with the ABAQUS 3D results. In particular the displacements (u, v, w) and all in-plane stresses (σ_x, σ_y, τ_{xy}) are in very good agreement with the maximum error
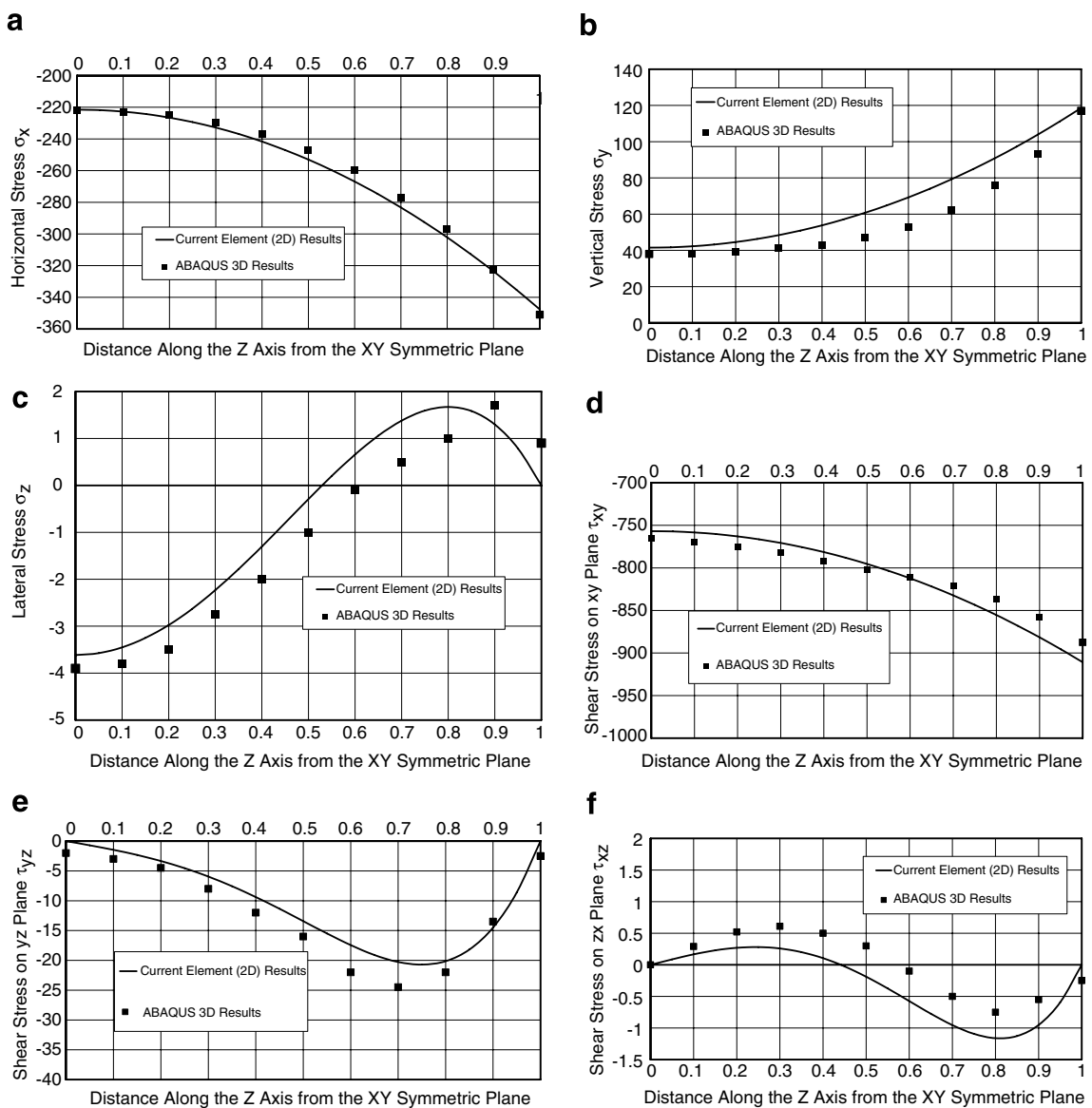

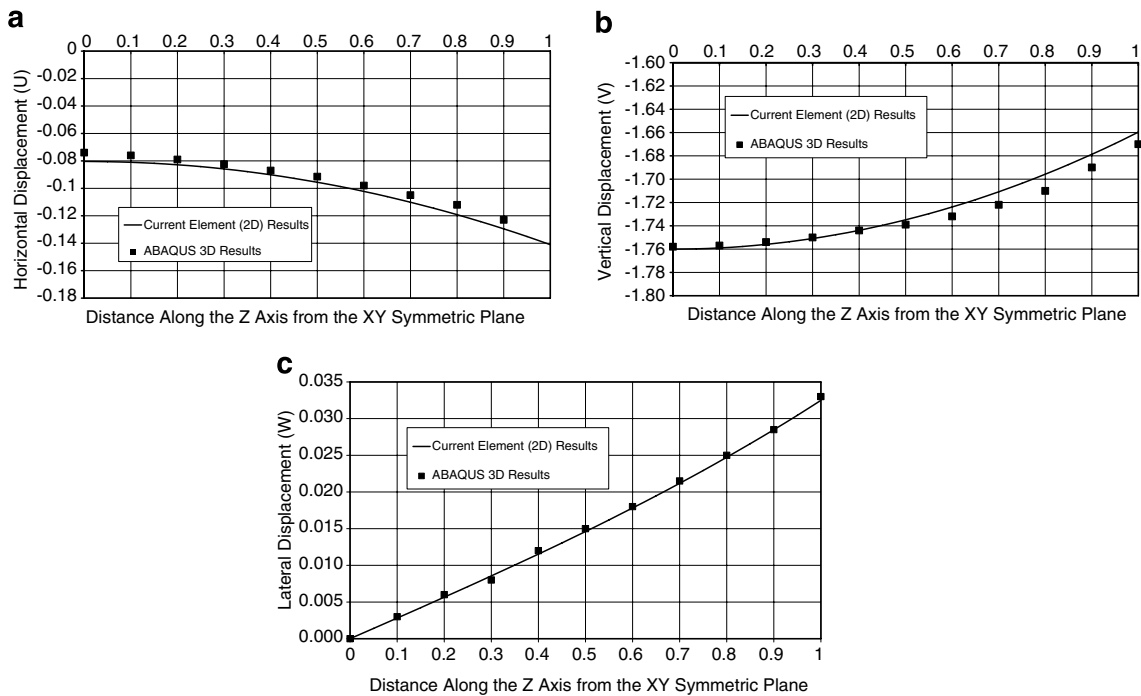Fig. 9. (a–f) Prediction of stresses for cube problem – Q3D24β element and ABAQUS.

Fig. 10. (a–c) Prediction of displacements for cube problem – Q3D24β element and ABAQUS.

less than 5%. As the lateral normal stress σ_z at the centre of the cube (location P in Fig. 10) is quite small (typically 0.9% of σ_x and 5% of σ_y), a new location (P' in Fig. 10) was chosen for validating the σ_z. It could be seen that the comparison is very good. Results predicted by the current elements may be viewed as the fitting of the corresponding results obtained by the 3D element in all these cases.

The two out-of-plane shear stresses (τ_{yz}, τ_{zx}) are very small (in particular the τ_{xz} being as small as 0.08% of τ_{xy}). At no other region of the body these stresses have been larger due to the type of problem considered. In spite of the small magnitude, the trend of the stress variations as predicted by ABAQUS and the Q3D24β element is in good agreement although the stress functions assumed for the out-of-plane shear in the current element formulation is somewhat more complex (this was required to eliminate the spurious deformation mode). Further refinement of the stress functions in the 2D formulation and/or meshing in the 3D analysis may eliminate the deviation in the magnitude of these two stress components.

8.2. Four block hollow masonry prism

Four block stack bonded hollow prisms were considered in the modelling. The clay blocks were nominally 150 mm × 310 mm × 76 mm in size and had two symmetrically placed voids of approximately 80 mm × 100 mm internal dimension. All prisms were constructed with 10 mm mortar joint. Face shell bedded mortar joint construction was considered. The prism was tested under uniform compression due to face shell loading. To examine the state of stress in the face shell bedded prism, prescribed vertical displacement ($v = -0.1$ mm) on the top surface was used.

Due to symmetry only a quarter of the prism was analysed. The mesh used in the analysis is shown in Fig. 11. The mesh consisted of solid and hollow elements. The solid Q3D24β element was used in the end web shell and the middle web shell. Full-bedded masonry prisms were modelled with solid elements for the portion of the mortar bed joints directly in contact with these two web shells and the top plywood capping. The face shell block and the associated mortar joints were modelled using hollow Q3D24βH elements. The model consisted of 88 elements and 108 nodes (648 degrees of freedom). The Young's modulus and
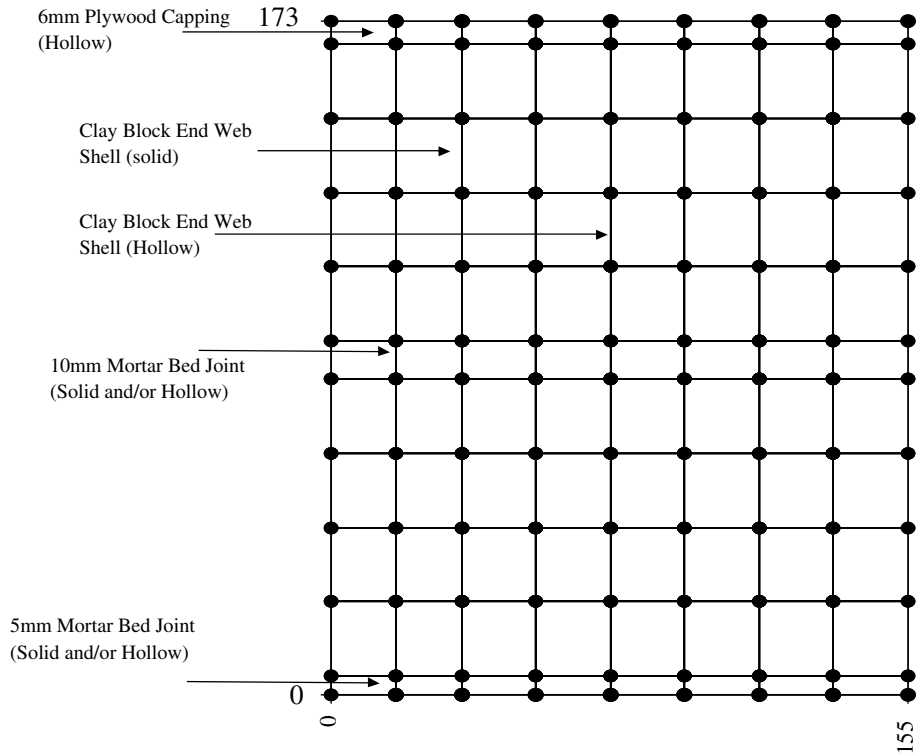
Fig. 11. Meshing of masonry prism using current elements Q3D24β and Q3D24βH.
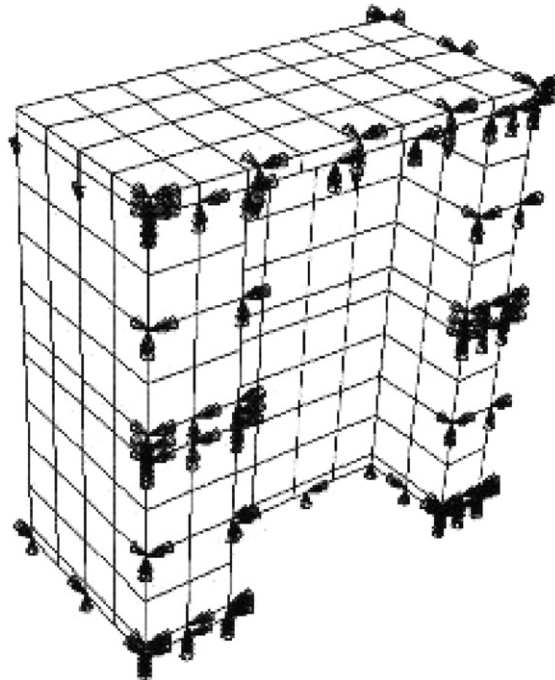

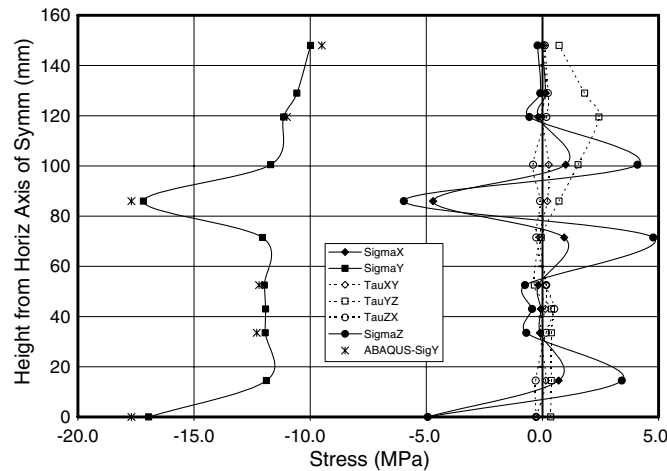Fig. 12. Meshing of masonry prism using 3D modelling in ABAQUS.

Fig. 13. Results of the analysis of masonry prism – current elements and ABAQUS.

the Poisson's ratio of the clay block, mortar and plywood capping were set as (35 GPa, 0.15), (5 GPa, 0.25) and (12 GPa, 0.12), respectively.

ABAQUS finite element package was used to validate the results. The hollow prism was modelled as a 3D assemblage of eight noded brick elements. A quarter model of the prism was analysed as shown in Fig. 12.

All components of stress at the midthickness of the end web shell ($x = 17.5$ mm $z = 0$ mm along y-axis) are shown in Fig. 13. The dominant vertical stress (σ_y) generated due to the application of a uniform prescribed vertical displacement of -0.1 mm was used to validate the 2D analysis result; the ABAQUS 3D modelling result is also shown in Fig. 13. The dominant σ_y stress predicted by the 2D analysis compare very well with the ABAQUS 3D analysis. All other stresses existed with their integral vanishing as exhibited by the distribution in Fig. 13.

It can be seen that the mortar joints are subjected higher levels of triaxial compression (σ_x, σ_y and σ_z) due to the lack of ability of the mortar to "spread" in the lateral direction due to incompatible deformation of the brick at the interface. This incompatible deformation modes at the interface induces lateral tension (σ_x and σ_z) in the web shells of the brick. There is much evidence in the literature that these stresses are the root cause of cracking of web shells of the face shell bedded prisms. The ability of the current Q3D24β and Q3D24βH elements to predict this complex phenomenon elegantly is worth noted.

9. Conclusions and discussions

Plane hybrid stress elements suitable for modelling solids and structural components of moderate thickness (or bodies whose dimensions are comparable to each other) with and without hollows where the classical plane stress and plane strain assumptions are either inadequate or inappropriate is presented in the paper. The geometry and loading of the solid/structure must be symmetric to its middle plane.

The elements exhibit very good convergence rate and they are not sensitive to the aspect ratio. The elements have been validated by comparing its results with that of the 3D elements (C3D8 and C3D8I) available in ABAQUS. All dominant displacement and stress fields have been predicted within good level of accuracy. The out-of-plane stresses were also predicted reasonably well.

The ability of the elements in predicting stresses in a face shell bedded masonry prism subjected to prescribed deformation with relative ease is considered important in the light of the complexity of such problems.

The behaviour of solids with moderate thickness differs from the plane stress and plane strain bodies particularly when the ratio of thickness to depth is between 1 and 10. It is, therefore, expected that this new element will find its applications in the inelastic and fracture mechanics based analysis of structural components with moderate thickness.

References

Afshari, F., Kaldjian, M.J., 1989. Finite element analysis of concrete masonry prisms. ACI Mater. J. 86, 525–530.

Broek, D., 1982. Elementary Fracture Mechanics, third ed. Martinus Nijhoff, Hague.

Dhanasekar, M., Xiao, Q.Z., 2001. Plane hybrid stress element method for 3D hollow bodies of uniform thickness. Comput. Struct. 79, 483–497.

Foster, S.J., Rangan, B.V., 1999. Finite element modelling of HSC squat walls in shear. In: Proc 16 ACMSM. AA Balkema, Sydney, pp. 115–120.

Pian, T.H.H., Sumihara, K., 1984. Rational approach for assumed stress finite elements. Int. J. Numer. Meth. Eng. 20, 1685–1695.

Pian, T.H.H., Wu, C.C., 1988. A rational approach for choosing stress terms for hybrid finite element formulations. Int. J. Numer. Meth. Eng. 26, 2331–2343.

Timoshenko, S.P., Goodier, J.N., 1970. Theory of Elasticity, third ed. McGraw-Hill.

Ugural, A.C., Fenster, S.K., 1995. Advanced Strength and Applied Elasticity. Prentice Hall, NJ.

Wu, C.C., Bufler, H., 1991. Multivariable finite elements: consistency and optimization. Sci. China (A) 34, 284–299.

Wu, C.C., Cheung, Y.K., 1995. On optimisation approaches of hybrid stress elements. Finite Elem. Anal. Des. 21, 111–128.

Wu, C.C., Pian, T.H.H., 1997. Numerical Analysis Method of Incompatible and Hybrid Elements. China Science Press (in Chinese).

Xiao, Q.Z., Karihaloo, B.L., Li, Z.R., Williams, F.W., 1999. An improved hybrid-stress element approach to torsion of shafts. Comput. Struct. 71, 535–563.

Ye, Z.M., 1997. A new finite element formulation for planar elastic deformation. Int. J. Numer. Meth. Eng. 40, 2579–2591.

Zhou, S., Hsieh, R., 1988. A thickness criterion for fracture toughness testing based on a plane stress compatible solution. Eng. Fract. Mech. 29, 41–47.